

## COMMUNICATION

[View Article Online](#)  
[View Journal](#) | [View Issue](#)

Cite this: *Dalton Trans.*, 2022, **51**, 10856

Received 10th April 2022,

Accepted 1st July 2022

DOI: 10.1039/d2dt01108e

[rsc.li/dalton](https://rsc.li/dalton)

# A microporous $Zr_6@Zr$ -MOF for the separation of Xe and Kr†

Fu-An Guo,‡ Kang Zhou,‡ Jiaqi Liu, Xingyu Li and Hao Wang \*

**We report here the self-assembly of a she-type zirconium-based metal–organic framework with discrete hexanuclear Zr-oxo clusters residing inside its pore windows. The overall structure features microporosity showing preferential adsorption of Xe over Kr.**

Metal–organic frameworks (MOFs) have attracted tremendous interest from scientific community over the past few decades because of their potential in a wide range of applications and their rich and diverse structural chemistry. Structural diversity of MOFs arises from theoretically countless combinations of metal nodes and organic struts, and tremendous variations of coordination/connection modes. Self-assembly of common metals and organic linkers into novel crystalline compounds would not only enrich the structural variety of MOFs, but the new materials may also exhibit excellent properties for certain applications.<sup>1–3</sup> To this end, the quest for novel MOF structures represents an important component of MOF research.

Gas separation represents one of the extensively investigated and the most fruitful areas of applications for MOFs as it benefits from their structural diversity and highly tunable pore shape/size and surface functionality.<sup>4–8</sup> Among various gas mixtures to be separated, noble gases represent the very challenging ones because of their inert nature. The separation of noble gases, especially Xe and Kr, is an important but challenging process to produce Xe with high purity.<sup>9</sup> Xe is used in a variety of applications, including commercial lighting, imaging, anaesthesia and insulation. Currently, cryogenic distillation is the most mature technology for separating Xe and Kr. The highly energy and capital intensive separation process and the low abundance of Xe make its price exceptionally

high. This has prompted the development of alternative technologies to achieve less energy-intensive, more cost-effective separation processes. Adsorptive separation by porous solids has attracted extensive attention in academia and industry because of its great potential in reducing energy consumption in chemical separation process. Various porous materials, such as MOFs, organic cages, zeolites, *etc.*, have been explored for the separation of Xe/Kr.<sup>10–14</sup> Among them, MOFs hold great promise as their nearly unlimited structures offer the opportunity for achieving high separation performance through structural regulation.

Here, we report a novel  $Zr_6@Zr$ -MOF structure (denoted as HIAM-401). The backbone network was constructed from a 6-connected  $Zr_6$  cluster and a 4-connected organic ligand, tetra (4-carboxylphenyl)ethylene (tcpe<sup>4–</sup>), featuring a **she** topology which has been commonly observed for Zr-MOFs built on planar tetracarboxylates.<sup>15,16</sup> This is different from the previously reported Zr-TCPE constructed from Zr and tcpe<sup>4–</sup>.<sup>17</sup> Interestingly, the pore windows of the cages in the **she** network are occupied by discrete, zero-dimensional hexanuclear Zr-oxo clusters. The  $Zr_6$  complexes are not removable through washing or solvent exchange with common organic solvents. However, they do not hinder the diffusion of small gases into the pores. The overall compound features microporosity and exhibits efficient separation of Xe and Kr under ambient conditions, with a Xe/Kr selectivity of 13 at 278 K and 1 bar for a typical binary mixture (Xe : Kr = 20 : 80).

Colourless block-shaped crystals of the title compound were obtained through a solvothermal reaction of  $H_4tcpe$  and  $ZrOCl_2 \cdot 8H_2O$  in acetic acid at 120 °C for 3 days. Single-crystal X-ray diffraction analysis indicated that the compound crystallizes in the cubic crystal system with a space group of  $Pm\bar{3}m$  (Table S1†). The backbone framework of HIAM-401 is formulated as  $Zr_6O_4(OH)_4(tcpe)_{1.5}(CH_3COO)_3(OH)_3(H_2O)_3$ . The network is built on a 6-connected hexanuclear zirconium-based SBU with 6 carboxylates surrounding the  $Zr_6$  core in a circle-shaped fashion. The other six connecting sites of the  $Zr_6$  SBU are occupied by terminal solvents ( $COOH^-$ ,  $OH^-$ ,  $H_2O$ ,

Hoffmann Institute of Advanced Materials, Shenzhen Polytechnic, 7098 Liuxian Blvd., Nanshan District, Shenzhen, Guangdong 518055, China.

E-mail: wanghao@szpt.edu.cn

†Electronic supplementary information (ESI) available. CCDC 2159612 and 2159615. For ESI and crystallographic data in CIF or other electronic format see DOI: <https://doi.org/10.1039/d2dt01108e>

‡These authors contributed equally to this work.

*etc.*). The SBUs are interconnected by  $\text{tcpe}^{4-}$  linkers to form the resulting three-dimensional (3D) network with the **she** topology (Fig. 1d and Fig. S1†). The framework features 3D pore systems consisting of large cages interconnected through relatively small windows. Interestingly, besides disordered free solvents inside the pores, a large number of discrete Zr-oxo clusters with the formula  $\text{Zr}_6\text{O}_4(\text{OH})_4(\text{CH}_3\text{COO})_4(\text{OH})_8(\text{H}_2\text{O})_8$  were observed residing at the pore windows, which are not chemically connected to the backbone framework. The ratio of the  $\text{Zr}_6$  SBUs in the network to the discrete ones is 8:3, with an occupancy of the latter being 74.1%. Thus the overall formula of HIAM-401 is  $[\text{Zr}_6\text{O}_4(\text{OH})_4(\text{tcpe})_{1.5}(\text{CH}_3\text{COO})_3(\text{OH})_3(\text{H}_2\text{O})_3]_8 \cdot 0.74[\text{Zr}_6\text{O}_4(\text{OH})_4(\text{CH}_3\text{COO})_4(\text{OH})_8(\text{H}_2\text{O})_8]_3$ . Although the windows of the 3D pores are occupied by the  $\text{Zr}_6$  clusters, the overall compound is still porous with regard to the crystal structure. There are one-dimensional (1D, interconnected to 3D) open channels with a diameter of around 1 nm. In addition, the large cages in the structure should be accessible to guest molecules as the occupancy of the  $\text{Zr}_6$  clusters is not approaching 100%. This could also be supported by the porosity analysis in the following discussion.

The phase purity of bulk HIAM-401 was confirmed by powder X-ray diffraction (PXRD) analysis (Fig. S2†). The pattern of the as-synthesized sample matches well with the theoretical one. It is noted that the crystallinity of the sample remained intact after being exposed to open air for two months, indicating its resistance to moisture. The thermogravimetric (TG) curve of the sample displays a weight loss of ~25% below 100 °C, followed by a plateau up to 500 °C (Fig. S3†). The permanent porosity of HIAM-401 was confirmed by  $\text{N}_2$  adsorption at 77 K on the ethanol-exchanged sample. It exhibited a typical type-I adsorption profile, with a saturated adsorption capacity of  $290 \text{ cm}^3 \text{ g}^{-1}$ , yielding a BET surface area of  $1029 \text{ m}^2 \text{ g}^{-1}$  and a pore volume of  $1.13 \text{ cc g}^{-1}$  (Fig. S5†). This indicates that the cages of the **she** network should at least be partially accessible to small gases. The adsorption-desorption isotherm of  $\text{N}_2$  at 77 K was collected twice consecutively and the two results are identical, suggesting the robustness of the compound.

An interesting question is whether the discrete  $\text{Zr}_6$  clusters in the structure of HIAM-401 remain intact during the washing and solvent exchange process or they would be washed out. To

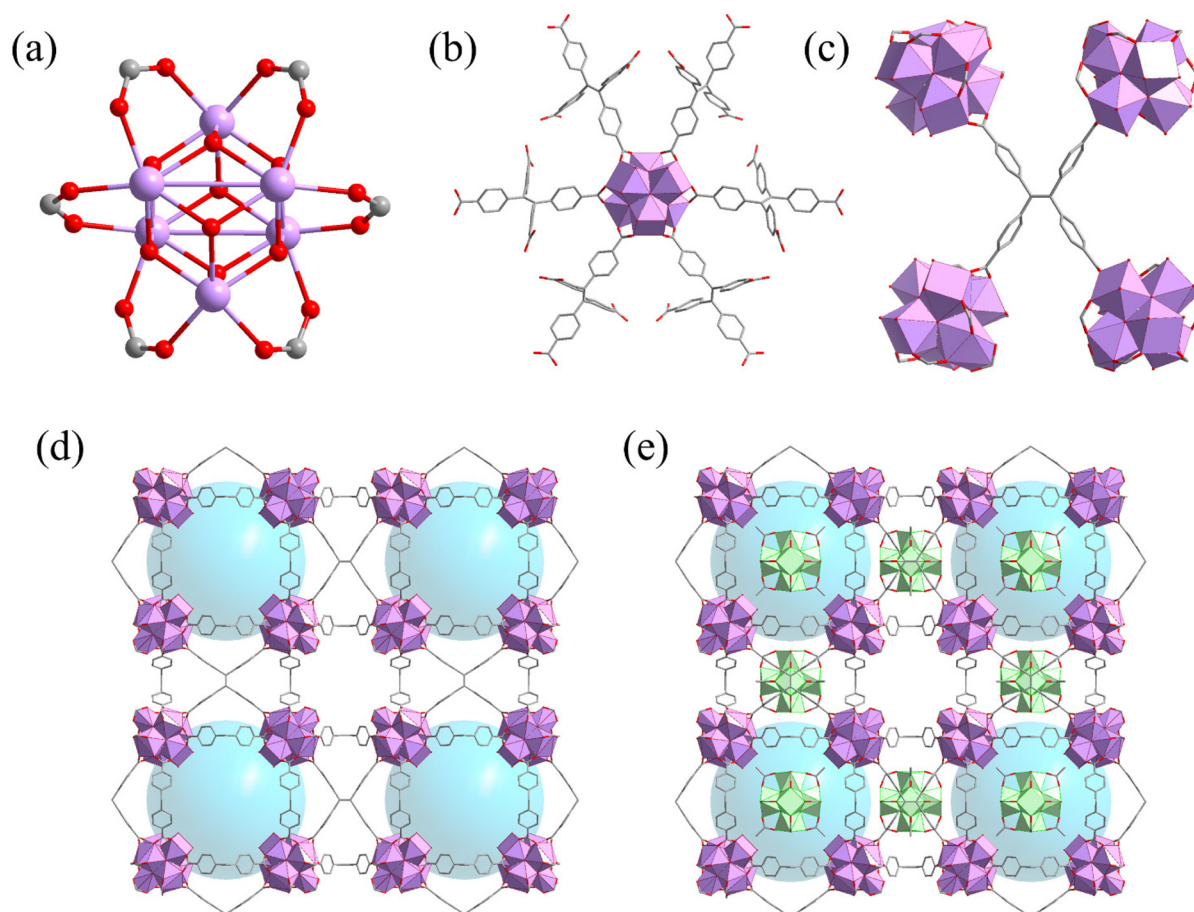


**Fig. 1** Crystal structure of HIAM-401. (a) and (b) Coordination environment of the hexanuclear SBU. (c) Connection mode of the organic linker  $\text{tcpe}^{4-}$ . (d) 3D structure representation of the backbone **she** network (cages are represented by hypothetical cyan balls). (e) The overall structure of HIAM-401. Color scheme: lavender: Zr in the backbone network, light green: Zr in the discrete clusters, red: O, grey: C. Hydrogen atoms and coordinated or free solvents are omitted for clarity.

find out the answer to this question, the crystals of the as-synthesized HIAM-401 were immersed in DMF and ethanol for 3 and 5 days, respectively. During the process each of the solvent was replaced daily. Fortunately, the crystallinity of the sample was fully retained upon washing and single crystal X-ray diffraction analysis was performed on the crystals afterwards (Table S1†). It was found that the overall connectivity of the structure was completely preserved, and no notable change in the backbone framework was observed. Importantly, the discrete  $\text{Zr}_6$  clusters remain residing at the same position in the pore without noticeable variations. The crystallographic ratio between the  $\text{Zr}_6$  in the backbone and the discrete  $\text{Zr}_6$  remains 8 : 3. It was noted that the occupancy of the discrete  $\text{Zr}_6$  clusters was slightly decreased to 70.7% from 74.1% of the original as-synthesized compound. Considering the possible variations of occupancy of the  $\text{Zr}_6$  clusters for different crystals, it is reasonable to conclude that the discrete  $\text{Zr}_6$  clusters would not be washed off by organic solvents and were largely retained in the subsequent adsorption process.

The compound was subsequently tested for the adsorption and separation of Xe and Kr. Single-component adsorption isotherms of Xe and Kr were collected at three different temperatures, 278, 288, and 298 K, up to 1 bar (Fig. 2a). The adsorption capacities for Xe are 66.5, 50.3, and 43.8  $\text{cm}^3 \text{g}^{-1}$  at 278, 288, and 298 K, respectively. In contrast, the uptake amounts for Kr are noticeably lower, with values of 19.1, 15.5, and 13.8  $\text{cm}^3 \text{g}^{-1}$  for 278, 288, and 298 K, respectively. The isosteric heats of

adsorption ( $Q_{\text{st}}$ ) for Xe and Kr were calculated from the adsorption isotherms at all three different temperatures, to evaluate their relative adsorption affinity. The  $Q_{\text{st}}$  value for Xe is 32.7  $\text{kJ mol}^{-1}$  at zero-coverage, which is among the highest values for the physisorption of Xe.<sup>9,18–20</sup> The value decreases slowly as a function of Xe loading, indicating that the Xe-framework interaction is stronger than that between the adsorbed Xe atoms. In contrast, the zero-coverage  $Q_{\text{st}}$  for Kr is 16.6  $\text{kJ mol}^{-1}$ , which is much lower compared to that of Xe. This confirms the favored adsorption for Xe over Kr by HIAM-401, which is consistent with the single-component adsorption isotherms that the adsorption capacities of Xe are notably higher than those of Kr.

To investigate the adsorption behavior of HIAM-401 for the mixed gases of Xe and Kr, ideal adsorbed solution theory (IAST) was used to determine its adsorption selectivity for a binary mixture of Xe : Kr = 20 : 80 at 278, 288, and 298 K (Fig. 3a). The ratio was selected in accordance with the typical composition of real industrial Xe/Kr mixtures. The Xe/Kr IAST selectivity of HIAM-401 approaches 19 at 278 K at low pressure and remains at  $\sim 13$  up to 1 bar. The value is higher than those of most reported MOFs including  $\text{Co}_3(\text{HCOO})_6$ ,<sup>21</sup> MOF-505,<sup>19</sup> MOF-74-Ni,<sup>22</sup> SBMOF-2<sup>23</sup> etc., but is lower than those of the recently reported  $\text{Co}_3(\text{C}_4\text{O}_4)_2(\text{OH})_2$ ,<sup>10</sup> CROFOUR-1-Ni<sup>24</sup> etc.<sup>9,11,20,25–28</sup> A trend of decreasing adsorption selectivity as a

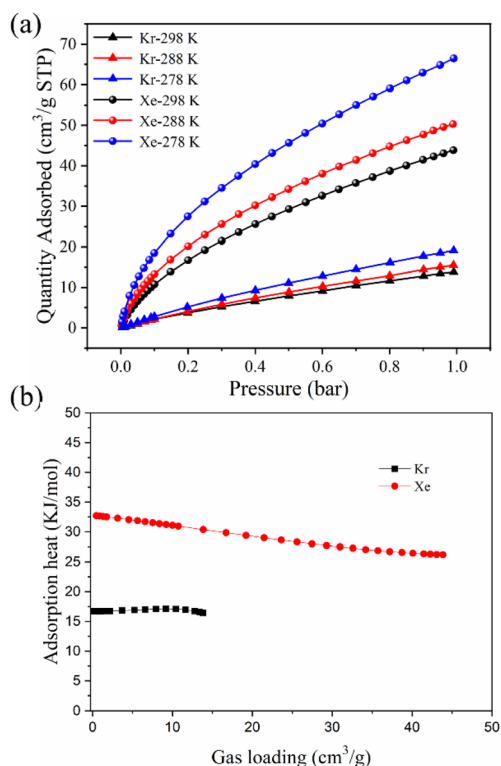


Fig. 2 (a) Adsorption isotherms of Xe and Kr at different temperatures; (b) heats of adsorption of Xe and Kr for HIAM-401.

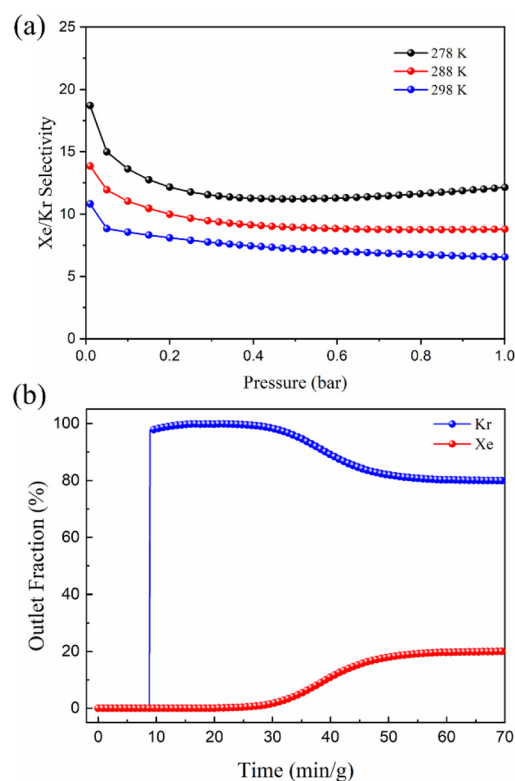


Fig. 3 (a) Calculated IAST selectivity for a binary Xe/Kr mixture (v/v = 20/80) at different temperatures. (b) Multicomponent column breakthrough curves with a feed of a binary Xe/Kr mixture (v/v = 20/80) for HIAM-401 at 298 K and 1 bar.

function of increasing temperature was observed. The Xe/Kr selectivity is around 7 at 298 K and 1 bar. In order to further evaluate the separation capability of HIAM-401 for Xe and Kr, experimental multicomponent column breakthrough measurements were performed using a Xe : Kr = 20 : 80 binary mixture as a feed. The breakthrough curve is displayed in Fig. 3b. Kr eluted out from the column first, at the 9th min  $\text{g}^{-1}$ . In contrast, Xe did not break out until the 27th minute. The notably longer retention for Xe than for Kr indicated that it was preferentially adsorbed by the adsorbent, consistent with the single-component adsorption results. The breakthrough experiments confirm that HIAM-401 is capable of separating Xe and Kr into pure individual components.

In summary, we report here the synthesis and characterization of an interesting  $\text{Zr}_6@ \text{ZrMOF}$  structure, HIAM-401. The 3D backbone network of the compound is built on 6-connected hexanuclear  $\text{Zr}_6$  SBUs, featuring a **she** topology. A large number of discrete  $\text{Zr}_6$ -oxo clusters reside at the pore windows of the **she** network which remain intact upon washing using common organic solvents. The overall structure of HIAM-401 remains microporous and shows selective adsorption of Xe over Kr. The adsorption selectivity and separation capability of the compound have been evaluated by IAST calculations and multicomponent column breakthrough measurements, respectively. This work may shed light on the development of more intriguing MOF structures which would largely enrich the structural diversity of MOFs.

## Conflicts of interest

There are no conflicts to declare.

## Acknowledgements

We are thankful for the financial support from the Natural Science Foundation of Guangdong Province (2019A1515010692) and National Natural Science Foundation of China (21901166).

## Notes and references

- X. L. Lv, L. Feng, L. H. Xie, T. He, W. Wu, K. Y. Wang, G. Si, B. Wang, J. R. Li and H. C. Zhou, *J. Am. Chem. Soc.*, 2021, **143**, 2784–2791.
- V. Guillermin and D. Maspoch, *J. Am. Chem. Soc.*, 2019, **141**, 16517–16538.
- L. Yu, S. Ullah, K. Zhou, Q. Xia, H. Wang, S. Tu, J. Huang, H.-L. Xia, X.-Y. Liu, T. Thonhauser and J. Li, *J. Am. Chem. Soc.*, 2022, **144**, 3766–3770.
- H. Furukawa, K. E. Cordova, M. O’Keeffe and O. M. Yaghi, *Science*, 2013, **341**, 1230444.
- A. H. Assen, Y. Belmabkhout, K. Adil, P. M. Bhatt, D.-X. Xue, H. Jiang and M. Eddaoudi, *Angew. Chem., Int. Ed.*, 2015, **54**, 14353–14358.
- H. Wang, X. Dong, V. Colombo, Q. Wang, Y. Liu, W. Liu, X.-L. Wang, X.-Y. Huang, D. M. Proserpio, A. Sironi, Y. Han and J. Li, *Adv. Mater.*, 2018, **30**, 1805088.
- H. Wang, Y. Liu and J. Li, *Adv. Mater.*, 2020, **32**, 2002603.
- A. Cadiau, K. Adil, P. M. Bhatt, Y. Belmabkhout and M. Eddaoudi, *Science*, 2016, **353**, 137.
- D. Banerjee, A. J. Cairns, J. Liu, R. K. Motkuri, S. K. Nune, C. A. Fernandez, R. Krishna, D. M. Strachan and P. K. Thallapally, *Acc. Chem. Res.*, 2015, **48**, 211–219.
- L. Li, L. Guo, Z. Zhang, Q. Yang, Y. Yang, Z. Bao, Q. Ren and J. Li, *J. Am. Chem. Soc.*, 2019, **141**, 9358–9364.
- J. Pei, X. W. Gu, C. C. Liang, B. Chen, B. Li and G. Qian, *J. Am. Chem. Soc.*, 2022, **144**(7), 3200–3209.
- H. Wang, Z. Shi, J. Yang, T. Sun, B. Rungtaweeworani, H. Lyu, Y. B. Zhang and O. M. Yaghi, *Angew. Chem., Int. Ed.*, 2021, **60**, 3417–3421.
- L. Wang, J. Ding, Y. Zhu, Z. Xu, Y. Fan, R. Krishna and F. Luo, *Microporous Mesoporous Mater.*, 2021, **326**, 111350.
- X. L. Wu, Z. J. Li, H. Zhou, G. Yang, X. Y. Liu, N. Qian, W. Wang, Y. S. Zeng, Z. H. Qian, X. X. Chu and W. Liu, *Inorg. Chem.*, 2021, **60**, 1506–1512.
- D. Feng, W.-C. Chung, Z. Wei, Z.-Y. Gu, H.-L. Jiang, Y.-P. Chen, D. J. Darensbourg and H.-C. Zhou, *J. Am. Chem. Soc.*, 2013, **135**, 17105–17110.
- J. S. Anderson, A. T. Gallagher, J. A. Mason and T. D. Harris, *J. Am. Chem. Soc.*, 2014, **136**, 16489–16492.
- S. Sun, C. Wei, Y. Xiao, G. Li and J. Zhang, *RSC Adv.*, 2020, **10**, 44912–44919.
- S.-J. Lee, K. C. Kim, T.-U. Yoon, M.-B. Kim and Y.-S. Bae, *Microporous Mesoporous Mater.*, 2016, **236**, 284–291.
- Y.-S. Bae, B. G. Hauser, Y. J. Colón, J. T. Hupp, O. K. Farha and R. Q. Snurr, *Microporous Mesoporous Mater.*, 2013, **169**, 176–179.
- D. Banerjee, C. M. Simon, S. K. Elsaidi, M. Haranczyk and P. K. Thallapally, *Chem*, 2018, **4**, 466–494.
- H. Wang, K. Yao, Z. Zhang, J. Jagiello, Q. Gong, Y. Han and J. Li, *Chem. Sci.*, 2014, **5**, 620–624.
- J. Liu, P. K. Thallapally and D. Strachan, *Langmuir*, 2012, **28**, 11584–11589.
- X. Chen, A. M. Plonka, D. Banerjee, R. Krishna, H. T. Schaefer, S. Ghose, P. K. Thallapally and J. B. Parise, *J. Am. Chem. Soc.*, 2015, **137**, 7007–7010.
- M. H. Mohamed, S. K. Elsaidi, T. Pham, K. A. Forrest, H. T. Schaefer, A. Hogan, L. Wojtas, W. Xu, B. Space, M. J. Zaworotko and P. K. Thallapally, *Angew. Chem., Int. Ed.*, 2016, **55**, 1–6.
- K. B. Idrees, Z. Chen, X. Zhang, M. R. Mian, R. J. Drout, T. Islamoglu and O. K. Farha, *Chem. Mater.*, 2020, **32**(9), 3776–3782.
- D. Banerjee, C. M. Simon, A. M. Plonka, R. K. Motkuri, J. Liu, X. Chen, B. Smit, J. B. Parise, M. Haranczyk and P. K. Thallapally, *Nat. Commun.*, 2016, **7**, ncomms11831.
- Y. Gong, Y. Tang, Z. Mao, X. Wu, Q. Liu, S. Hu, S. Xiong and X. Wang, *J. Mater. Chem. A*, 2018, **6**, 13696–13704.
- K. B. Idrees, Z. Chen, X. Zhang, M. R. Mian, R. J. Drout, T. Islamoglu and O. K. Farha, *Chem. Mater.*, 2020, **32**, 3776–3782.